LBL-27523
Preprint

Lawrence Berkeley Laboratory
UNIVERSITY OF CALIFORNIA

Submitted to International Journal of Radiation Oncology, Biology, Physics

Image Correlation of MRI and CT in the Treatment Planning for Radiosurgery of Intracranial Vascular Malformations

M.H. Phillips, M. Kessler, F.Y.S. Chuang, K.A. Frankel, J.T. Lyman, J.I. Fabrikant, and R.P. Levy

July 1989

Donner Laboratory

Biology & Medicine Division

Prepared for the U.S. Department of Energy under Contract Number DE-AC03-76SF00098.

DISCLAIMER

IMAGE CORRELATION OF MRI AND CT IN THE TREATMENT PLANNING FOR RADIOSURGERY OF INTRACRANIAL VASCULAR MALFORMATIONS[1]

Mark H. Phillips
Marc Kessler
Frank Y.S. Chuang
Kenneth A. Frankel
John T. Lyman
Jacob I. Fabrikant
Richard P. Levy

Research Medicine and Radiation Biophysics,
1 Cyclotron Road
Lawrence Berkeley Laboratory
Berkeley, CA 94720

July 18, 1989

[1]This research was supported by the Office of Health and Environmental Research, U.S. Department of Energy contract DE-AC03-76SF00098.

Abstract

Magnetic resonance imaging (MRI) has been incorporated with stereotactic cerebral angiography and computed tomography (CT) in the treatment planning process of heavy ion radiosurgery of intracranial arteriovenous malformations (AVMs). Correlation of the images of the AVM and normal tissue on each of these neuroradiological imaging modalities is achieved by means of fiducial markers. The computerized transfer of angiographic information to the CT images regarding the size, shape, and location of the abnormal vasculature has been described in an earlier report. A separate computer program calculates a fit between individual fiducial markers on the CT and MR images that enables the transfer of contours between the two imaging modalities. The goodness of fit is determined by contouring features easily recognizable on both sets of images and comparing them. The MRI images aid in the determination of the three-dimensional shape of the AVM, adding to the information derived from the two angiographic projections. Currently, MRI cannot replace cerebral angiography in delineating the entire, arterial phase of the AVM. MRI is invaluable in the treatment planning of angiographically-occult AVMs, determining the location, size, and shape of the volume to be treated. Correlation of the CT and MRI images allows for the transfer of CT-calculated isodose contours to the MRI images to aid in the determination of optimal treatment plans.

Key Words: stereotactic radiosurgery, charged particles, AVM, magnetic resonance. treatment planning

INTRODUCTION

The development of nuclear magnetic resonance imaging (MRI) has greatly enhanced the ability to image anatomical structures and pathological states. In the brain, critical structures such as the pons, midbrain and the thalamus are easily visible, and the gray and white matter components of brain tissue can be distinguished. Normal vasculature is not normally imaged (with the exception of the large vessels, such as the carotids), but regions of high or low flow rate can be enhanced with suitable pulse sequences [11]. The abnormal vasculature of intracranial arteriovenous malformations (AVMs) is most often seen as a flow void when there are large numbers of vessels or large distended feeding and draining vessels [6,14]. AVMs that have clinically demonstrable effects, yet are angiographically-occult ("cryptic"), are imaged by magnetic resonance. Cryptic AVMs have characteristic MR images due to hemorrhage-induced changes that have proven to be good predictors of the angiographic appearance [7,15]. In addition to imaging the AVM, MRI demonstrates the location of hemorrhage, both acute and chronic [1,15].

These advances have resulted in MRI studies becoming part of the standard neuroradiological imaging work-up for the diagnosis and treatment planning of intracranial AVMs, in concert with cerebral angiography and x-ray computed tomography (CT). Angiography's ability to image the hemodynamics of the AVM by following the passage of a bolus of contrast medium from the arterial to the venous phase, along with its high spatial resolution, makes it the standard imaging procedure [14]. Contrast-enhanced CT demonstrates the region containing the nidus and the large feeding draining vessels, and, in the case of cryptic AVMs, regions of slowly flowing blood [6,14]. Non-contrast CT is used in the treatment planning calculations [13] and for the diagnosis of acute hemorrhages.

The radiosurgical treatment of AVMs is based on the delivery of a uniform radiation dose to the arterial component of the lesion while attempting to spare

the venous structures, damage to which could compromise normal tissue [3,4,8,9]. In this paper, we describe the integration of MRI into the treatment planning procedure, and the impact it has had in the radiosurgical treatment of intracranial AVMs.

METHOD AND MATERIALS

All patients admitted to the radiosurgical protocol at Lawrence Berkeley Laboratory (LBL) undergo stereotactic cerebral angiography (with the exception of those patients with cryptic AVMs who do not undergo angiography), CT, and MRI. The neuroradiological procedures are performed with the patient fixed in the stereotactic frame and removable mask system, as described in Ref. [10]. The patient wears a mask constructed of thermoplastic that conforms very accurately to the contours of the head. This mask is mounted in a versatile, lightweight frame that defines a fixed reference frame by means of a series of fiducial markers. Specially-designed interfaces are used to mount the stereotactic frame on the angiography unit, the CT unit, and the radiosurgical treatment couch. The MRI frame is identical to the frame used in the x-ray studies in all important dimensions and is constructed of lucite and nylon; the metal fiducial markers and positioning pins have been replaced with non-metallic ones.

To integrate the information from CT and MRI, a set of approximately 12 point-like fiducial markers is fixed to the patient mask. For MRI, each marker is approximately 1.5 mm in diameter; these small beads are fabricated by filling plastic tubing with olive oil and sealing the ends with a heated clamp. For CT, 1 mm diameter bits of solder are used. They are widely distributed about the mask to ensure visualization in the different imaging planes.

The MRI procedures are conducted at several different facilities, and two different imaging systems are used. [2] Imaging sequences are performed in three

[2]GE Signa MR Scanner, General Electric Company, Milwaukee, WI (1.5 Tesla) and the LBL-

orthogonal planes-axial, sagittal, and coronal. The slice thickness is 5 mm, and the slices are either interleaved using two scan sequences or are separated by 6 mm using one scan sequence. Typically, a sagittal sequence is taken first to localize the lesion. This is followed by an axial series and a coronal series. The axial series is the most extensive spatially, usually encompassing nearly the entire skull. The sagittal series usually covers somewhat more than half the skull, and the coronal series is typically limited to the planes immediately adjacent to and intersecting the lesion.

The axial series has a long T_R (2000 msec) and short T_E (20/80 msec, first and second echo); the sagittal typically has T_R of 800 msec and a T_E of 20 msec; and the coronal has a T_R of 600 msec and a T_E of 20 msec. These are typical clinically-used scan parameters for the diagnosis of such lesions. The slice spacing is somewhat closer than normal to ensure that the entire AVM, as well as all the fiducial markers, is adequately imaged for treatment planning purposes.

The resulting sets of images are recorded in digitized form on magnetic tape for transfer to the treatment planning computer. After transfer, each image is scrutinized, the x, y, and z coordinates of each fiducial marker are recorded on both the MRI and CT data sets, and a least-squares fit between the MRI coordinates and the CT coordinates is calculated. The fit parameters can be calculated between the axial CT slices and each set of MRI slices– axial, sagittal and coronal. Once the fit is determined, any set of points on one image set can be transformed to the coordinate space of any other image set.

The computer modeling and algorithms used to carry out the image correlation between CT and MR images are described fully in Ref. [5]. A set of contours that define a volume in either CT or MR space is modeled as a surface by means of a tiling algorithm which joins sets of adjacent points. The node points that determine the surface are multiplied by the transformation matrix to produce a surface in the

MIT-IBM MRI unit (0.5 Tesla).

reference frame of the corresponding imaging modality. The orientation of the image planes in this modality are calculated, the three-dimensional surface is sliced along these planes, and the appropriate points defining the contour in this plane are determined.

To determine the goodness of fit of the correlation, several structures that are easily identified on both CT and MRI are contoured, transformed, and viewed. Typically, the pituitary and the inner table of the skull are used for this purpose. If the AVM has not been imaged angiographically, the accuracy of the correlation between the angiographic films, CT and MRI is checked. (Ref. [13] describes how the angiographic information is transferred to the CT images.) By careful construction of the frame-couch interfaces, and use of the patient mask, the orientation of the slices is generally very similar between different studies. Differences are corrected by application of the least squares fitting procedure. The transformation calculated in the fitting procedure contains the translation vector and the scaling and rotation matrix between the reference frames defined by each imaging procedure.

The AVM is then viewed in all three planes of the MR images and target contours drawn. These contours are then transformed to the CT images. They are compared with the angiographically-derived contours. For cryptic AVMs, the MR contours are used to define the AVM volume. Using these target contours, a treatment plan is calculated [2,13], and a set of isodose contours on the appropriate CT slices is obtained. These isodose contours are then transformed to MRI coordinates so that the isodose distributions can be viewed overlaid on the MR images. Correlations between CT and coronal MR images have been performed only in a few cases due to the relatively small number of slices typically imaged and the subsequent difficulty in visualizing sufficient fiducial markers to obtain a good fit.

RESULTS

Correlations between MRI and CT have been calculated for 36 patients with arteriovenous malformations. Of these, 11 were diagnosed as having cryptic AVMs. The results of the correlations have been used in a progressive fashion to improve the technique of patient-mask making, to optimize the positioning and construction of the fiducial markers, and to alter the interfaces between the diagnostic equipment patient couches and the stereotactic frame to achieve reliable and accurate patient repositioning within the mask.

The patient mask is designed to reliably reposition the patient's head for each imaging study. The correlation of MRI and CT images provides the opportunity to measure the positioning reproducibility, as demonstrated in Fig. 1. The inner table of the skull was contoured on each axial CT slice, spanning the entire head. This volume was transformed to both the axial and sagittal MR image spaces, sliced along the planes corresponding to the MR images, and the resulting contours displayed on the corresponding MR images. This procedure is capable of detecting small rotations, as well as translations, between the two imaging procedures. In the MR sagittal view, a small portion of brain tissue can be seen extending beyond the superior portion of the inner table contour. This is a result of the volume averaging and resultant uncertainty in contour position that results from the finite CT slice thickness (5 mm thick with 3 mm spacing) in a region of sharply sloping bone-soft tissue interface.

The verification procedures described above and illustrated in Fig. 1 are necessary to determine whether the calculated transformation is correct. With a satisfactory fit, the AVM contours derived from the angiographic procedure are transformed into the MR image space. Figures 2 – 4 illustrate examples of AVMs visualized by cerebral angiography which are then transferred to the appropriate CT and MR images. In figure 2, the angiographic contour corresponds very well to the region of

abnormal vasculature visible on the MR image. In figure 3, the correspondence is not as good, due to the presence of large feeding arteries and draining veins, and a region of small, filamentous vessels. The large veins are not included as part of the angiographic contour, since the radiosurgical treatment targets the arterial phase of the AVM. However, the exact locations of the large veins relative to the tangled masses of vessels within the AVM nidus are not easily determined on the MR images, as both groups of vessels cause flow voids and the nuclear magnetic resonance technique is unable to distinguish the arterial and venous phases. The region of small, filamentous vessels visible on the angiographic image does not provide enough contrast in the MR image to be visualized. An example of a case wherein the MR images were used to resolve an ambiguity in the shape of the AVM is demonstrated in Figure 4. The AVM as seen on the AP and lateral projections of the cerebral angiogram is outlined in (a) and (b). These contours, after transformation to the MR study, are shown on axial and sagittal MR images. The abnormal vasculature of the AVM is visible on the MR image as a region of low signal intensity. This region differs somewhat from the angiography-derived contours due to the fact that the two angiographic projections do not contain the full, three-dimensional information. A small projection of abnormal vasculature on angiographic projections results in the formation of CT contours that contain appreciable volumes of normal tissue because the two dimensional projections do not contain full volume information.

Figure 5 illustrates the use of MRI in the treatment planning of cryptic AVMs. Cerebral angiography of this lesion revealed no abnormal vasculature, yet the patient suffered intracranial hemorrhage from the lesion, which was demonstrated on CT. The lesion was visible on the MR image as a region of hyper-intensity in the pons, surrounded by regions of hypo-intensity. The region to be treated was contoured on the MR images, and the contours transformed to the CT images.

Figure 6 shows a three-dimensional treatment plan as calculated on the CT

slices (axial and sagittal) passing through the center of the lesion. Isodose contours are shown for the 90, 70, 30, and 10% of the dose. Four beam directions were used: one posterior beam angled 30° superiorly, one posterior beam angled 5° inferiorly, one lateral beam angled 25° posteriorly, and one oblique beam directly above the third beam 30°. These contours are also shown on the corresponding axial and sagittal MR images. The dose to particular anatomical stuctures that are imaged with MR can be easily seen and aids in decisions regarding a particular treatment plan.

DISCUSSION

At LBL, the integration of different imaging modalities has proven to be an important element in the radiosurgical treatment of arteriovenous malformations using monoenergetic beams of helium ions. MRI has several definite roles to play in the treatment planning of these vascular disorders, each role exhibiting strengths and weaknesses inherent in the method and dependent on the exact nature of the lesion to be treated.

The accuracy of the correlations between the CT, MRI, and cerebral angiography images is a crucial element in the effectiveness of the treatment planning procedures. The effectiveness of the stereotactic frame and mask and the accuracy of the correlation between CT and angiography have already been discussed in earlier reports [10,13]. However, the incorporation of MRI has resulted in some slight modification of our procedures, a better understanding of the source and magnitude of errors in the repositioning of the patient within the mask, and an increased confidence in the accuracy of our ability to target and irradiate a desired volume of tissue within the brain. The three-dimensional matrices of information provided by CT and MRI yield more detailed images for comparison than the projected views of stereotactic angiography. Such comparisons indicated that the major source of

error between separate studies was rotation about the left-right axis of the head. Increased attention to the fitting of the mask and adjustments in the frame-patient couch interfaces on the separate imaging systems have reduced this problem.

The correlations between CT and the axial MR images and the sagittal MR images are usually the poorest along the axis perpendicular to the plane of the image. Within the plane of the image, the position of the fiducial markers can be determined to the resolution of the image, approximately 1 mm. In the direction perpendicular to the images, the slice thickness significantly affects the resolution. For CT, 5 mm thick slices with 3 mm separation are typically used, and for MRI, 5 mm thick slices with 6 mm slice separation are used. It is not unusual for the transformation between axial MRI to axial CT to be incorrect by approximately one CT slice. In these cases, examination of the images is used to alter the transformation matrix and effect a more accurate correlation. Volume-averaging in the MR images can also be significant when contouring a small volume and transforming the contours to CT images.

The first stage of treatment planning is to define the target. As illustrated in Fig. 2–4, magnetic resonance images contain a wide range of information with regard to delineating the exact contours of the abnormal vasculature. Examples are given that illustrate good agreement between MRI and angiography, poor agreement where angiography is superior, and poor agreement where MRI is superior. In our system that uses two orthogonal angiographic projections to define the target contours, the three-dimensional information in MRI is most helpful when a small projection of abnormal vasculature distorts the dimensions of the projected lesion, with the result that an appreciable volume of normal tissue is included in the target volume (Fig. 4). MRI can also prove useful in clearly imaging the architecture of the brain, so that functional structures can be distinguished. Although CT has some use here as well, MRI has much better contrast, and the determination of

the volume to be included in the high dose region can take into account information detailing the degree to which the AVM has invaded or distorted the normal architecture of the healthy brain tissue [6]. In our experience, MR studies that provide information resulting in modifications to the angiographically-derived contours occur in approximately one-quarter to one-third of the cases.

Figure 3 illustrates a case wherein the MR images appear to be unhelpful in defining the nidus of the AVM when compared to cerebral angiography. Such poor agreement between these imaging modalities is most common in large AVMs, where large volumes of blood are shunted through the AVM into large, draining veins. MRI might appear, at first glance, to suffer in the comparison for such lesions. In fact, the magnitude of the shunt in these cases often means that the arterial and venous phases are not clearly delineated on angiography, and the distended draining veins can impair visualization of the arterial component when projected onto the plane of the x-ray film. Although it is not easy to visualize in the photographs of the MR images in Fig. 3, the large venous draining veins are often distinguishable from the arterial component by virtue of the uniform intensity of the flow void of the veins and the ability to image sequential slices so that the spatial course of the vein can be followed as different levels within the brain are viewed. This ability to use the three-dimensional information to help define the nidus often results in measured AVM dimensions that are smaller when measured on MRI than on angiography [12]. However, in many of these cases, the arterial phase is inextricably tangled with the venous structures and it is not possible to define a target for radiosurgery that would exclude only the latter. This additional three-dimensional information can be useful in the assessment of the prognosis for treatment and in intepreting subsequent neuroradiological imaging procedures to follow radiation-induced changes, but, in general, it is not helpful in determining the target volume.

Similar conclusions concerning the relative roles of MRI, CT and cerebral

angiography in determining the size and location of AVMs have resulted from other studies designed to evaluate the role of the imaging modalities in the management of these lesions [6,14]. It should be noted that the figure stated above for the fraction of cases in which MRI has provided additional, useful information in determining the region to be treated may be skewed with respect to the general AVM population presenting for radiosurgical treatment. Heavy charged particle radiosurgery has proven to be exceptionally capable of treating large AVMs with the result that the median size of AVM treated at LBL is 4 cm^3. As described above, MRI is less likely to image clearly the AVM nidus when the lesion is large than when it is small.

MRI has proven invaluable in the treatment planning of cryptic AVMs. These lesions, while not visualized by cerebral angiography, have demonstrable effects as a result of acute or chronic hemorrhage, particularly when located in critical areas such as the brainstem. CT with contrast can image the AVM in some cases. However, the precise region to be irradiated is not always clear due to the presence of calcium resulting from previous hemorrhage, and artifacts due to dense bone in the case of lesions in the lower brainstem. The specificity of MRI in imaging regions of hemorrhage, and the imaging of the AVM in the sagittal and coronal planes, provide much better information than CT in determining aperture shapes and compensation for charged particle treatment. The use of MRI in the treatment planning of cryptic AVMs has resulted in much better localization of the target and shaping of the high dose region, which is of great importance when these lesions are located in the most sensitive regions of the brain.

The treatment planning calculations require data detailing the physical characteristics of the tissue to be traversed by the charged particles, as well as the shape and location of the target volume. The former is needed to calculate the residual range of the particles in order that the distal edge of the Bragg peak falls on the distal boundaries of the target; the latter is needed to accurately shape the beam

by means of beamshaping apertures, compensation, and spreading of the Bragg peak. The range calculations rely on a calibration curve that converts x-ray attenuation coefficients measured by CT to charged particle stopping powers [2]. The dependence of the measured MRI signal on the exact pulse sequence and tuning parameters makes these data unsuitable for use in the accurate calculations of residual range even if some sort of calibration curve could be devised.

The major role of MRI in the treatment planning calculations, aside from the determination of target shape and location, lies in its ability to image clearly details of brain architecture. The determination of beamport orientation, number, and weighting must take into account the resultant dose distribution and the regions of normal tissue likely to be affected. Once the transformations between the MR image set and the CT image set have been calculated, both target contours and isodose contours can be transferred. Calculations of the isodose contours performed on CT images are transferred to the magnetic resonance images in order to assess the risk to particular anatomical structures within the brain. These examinations of dose distributions on MRI are most useful for lesions located in or near the brainstem and thalamus, where the sharp dose fall-off characteristic of charged particles can be used to advantage. Of the patients on whom image correlation studies have been performed, 12 had AVMs located in the brainstem.

Another aspect of MRI that is of interest in the treatment of vascular lesions is the development of MRI angiography, that is, fast, flow-sensitive imaging sequences. To date, these methods have produced some impressive images, particularly when integrated with three-dimensional viewing capabilities. However, the inability to separate the arterial and venous phases makes it unlikely that such images will replace conventional cerebral angiography.

SUMMARY AND CONCLUSIONS

Magnetic resonance imaging has been incorporated in several ways into the treatment planning of heavy charged particle radiosurgery of intracranial arteriovenous malformations. It is used to aid in the determination of the exact boundaries of the volume to be treated with a uniform dose of radiation. In this role, MRI has proven most helpful in those cases where the AVM is irregularly shaped, where large, venous structures are intertwined with the AVM nidus, and where the AVM is angiographically-occult. The major limitation of MRI in delineating the region to be treated is its inability to distinguish the arterial from the venous components of the AVM. The second role of MRI is to exploit MRI's excellent imaging capabilities of the structural features within the brain. By overlaying the CT-calculated isodose contours on the MR images, the decisions on the orientation and number of beamports to be used can be made to optimize the dose delivered to the target volume while attempting to minimize normal tissue injury.

Acknowledgements

We would like to gratefully acknowledge the helpful discussions with Drs. Dieter Enzmann, Robert DeLaPaz and Michael Marks of the Stanford University Medical Center. The cooperation and suggestions of the entire staff at the Stanford University Advanced Imaging Center greatly facilitated our work and made it much more enjoyable. We would also like to acknowledge the work of Dr. Samuel Pitluck, Terri Whitcomb, and James Judnick for their help in computer programming and imaging studies.

Bibliography

[1] Atlas, S.W.; Mark, A.S.; Grossman, R.I.; Gomori, J.M. Intracranial hemorrhage: gradient-echo MR imaging at 1.5 T. *Radiology*, **168**: 803-807; 1988.

[2] Chen, G.T.Y.; Singh, R.P.; Castro, J.R.C.; Lyman, J.T.; Quivey, J.M. Treatment planning for heavy ion radiotherapy, *Int J Radiat Oncol Biol Phys*, **5**: 1809-1809; 1979.

[3] Fabrikant, J.I.; Frankel, K.A.; Phillips, M.H.; Levy, R.P. Stereotactic heavy charged-particle Bragg peak radiosurgery for intracranial arteriovenous malformations, In Edwards, M.S.B. and Hoffman, H.J., editors, *Cerebral Vascular Diseases of Childhood and Adolescence*, chapter 22, Part 2, Williams and Wilkins, 1988.

[4] Fabrikant, J.I.; Lyman, J.T.; Hosobuchi, Y. Stereotactic heavy-ion Bragg peak radiosurgery: method for treatment of deep arteriovenous malformations, *Br J Radiol*, **57**: 479-490; 1984.

[5] Kessler, M.L. Integration of multimodality imaging data for radiotherapy treatment planning. Thesis (Ph.D.), University of California, Berkeley, CA; May, 1989.

[6] Leblanc, R.; Levesque, M.; Comair, Y.; Ethier, R. Magnetic resonance imaging of cerebral arteriovenous malformations, *Neurosurgery*, **21**: 15-20; 1987.

[7] Lemme-Plaghos, L; Kucharczyk W.; Brant-Zawadski, M.; Uske, A.; Edwards, M.; Norman, D.; Newton, T.H.. MRI of angiographically occult vascular malformations, *AJR*, **146**: 1223-1228; 1986.

[8] Levy, R.P.; Fabrikant, J.I.; Frankel, K.A.; Phillips, M.H.; Lyman, J.T. Stereotactic heavy-charged-particle Bragg peak radiosurgery for the treatment of intracranial arteriovenous malformations in childhood and adolescence, escence. *Neurosurgery*, **24**: 841-852, 1989.

[9] Lyman, J.T.; Kanstein, L.; Yeater, F.; Fabrikant, J.I.; Frankel, K.A. A helium-ion beam for stereotactic radiosurgery of central nervous system disorders, *Med Phys*, **13**: 695-699; 1986.

[10] Lyman, J.T.; Phillips, M.H.; Frankel, K.A.; Fabrikant, J.I. Stereotactic frame for neuroradiology and charged particle Bragg peak radiosurgery of intracranial disorders, *Int J Radiat Oncol Biol Phys*, **16**: 1989.

[11] Needell, W.M.; Maravilla, K.R. MR flow imaging in vascular malformations using gradient recalled acquisition, *AJNR*, **9**: 637-642; 1988.

[12] Noorbehesht, B.; Fabrikant, J.I.; Enzmann, D.R. Size determination of supratentorial arteriovenous malformations by MR, CT and Angio. *Neuroradiology*, **29**: 512-518; 1987.

[13] Phillips, M.H.; Frankel, K.A.; Lyman, J.T.; Fabrikant, J.I.; Levy, R.P. Heavy charged-particle stereotactic radiosurgery: cerebral angiography and CT in the treatment of intracranial vascular malformations, *Int J Radiat Oncol Biol Phys*. In press; 1989.

[14] Smith, H.J.; Strother, C.M.; Kikuchi, Y.; Duff, T.; Ramirez, L.; Merless, A; Toutant, S. MR imaging in the management of supratentorial intracranial AVMs, *AJNR*, *9*: 225-235; 1988.

[15] Sze, G.; Krol, G.; Olsen, W.L.; Harper, P.S.; Galicich, J.H.; Heier, L.A.; Zimmerman, R.D.; Deck, M.D.F. Hemorrhagic neoplasms: MR mimics of occult vascular malformations, *AJR*, **149**: 1223-1230; 1987.

Figure Captions

Figure 1: Upper left: Axial CT image with contours (white dots) drawn delineating the pituitary and the inner table of the skull. Upper right: Axial MR image corresponding the CT image. The contour surrounding the pituitary has been tranformed from the CT images using image correlation techniques. Lower left: Axial MR image with CT-derived inner table contour shown. Lower right: Sagittal MR image with inner table contours drawn on axial CT images and transformed.

Figure 2: Upper and lower left: AP and lateral internal carotid injections demonstrating a 2.5 cm^3 AVM located in the temporal lobe of a 26 y old female. Upper right: axial and sagittal MR images through the AVM with the contours of the AVM as defined by angiography delineated by the white dots.

Figure 3: Upper and lower left: AP and lateral internal carotid injections demonstrating a 45 cm^3 AVM located in the basal ganglia and thalamus of a 21 y old male. Upper and lower right: 2 axial MR images through different parts of the AVM. The angiographically-defined contours of the AVM are illustrated. Hypointense regions of the image correspond to flow voids resulting from large feeding and draining vessels.

Figure 4: Upper and lower left: AP and lateral internal carotid injections demonstrating a 18 cm^3 AVM located in the thalamus and internal capsule of a 14 y old male. Upper and lower right: axial and sagittal MR images through the AVM with the angiographically-defined AVM contours illustrated. Regions of normal brain tissue can be seen to be included with the region bounded by the angiographically-defined contours.

Figure 5: CT and MR images of a angiographically-occult AVM located in the pons of a 28 y old female. The white contours outline the region to be treated as defined by the axial (upper right) and sagittal (lower right) MR views. The axial MR contours were transformed to CT image space and displayed on the axial CT

image (upper left). The CT was performed without contrast; the window and level of the image are adjusted so that calcification resulting from previous hemorrhages is visible within the MRI-derived contours.

Figure 6: The same patient as shown in Fig. 5. A three-dimensional dose distribution was calculated on the CT images using the MRI-derived AVM contours. Isodose lines are shown for the 90, 70, 50, and 10% dose levels on the axial (upper left) and sagittal (lower left) CT images. The isodose contours were transformed to MRI space and displayed on the axial (upper right) and sagittal (lower right) MR images.

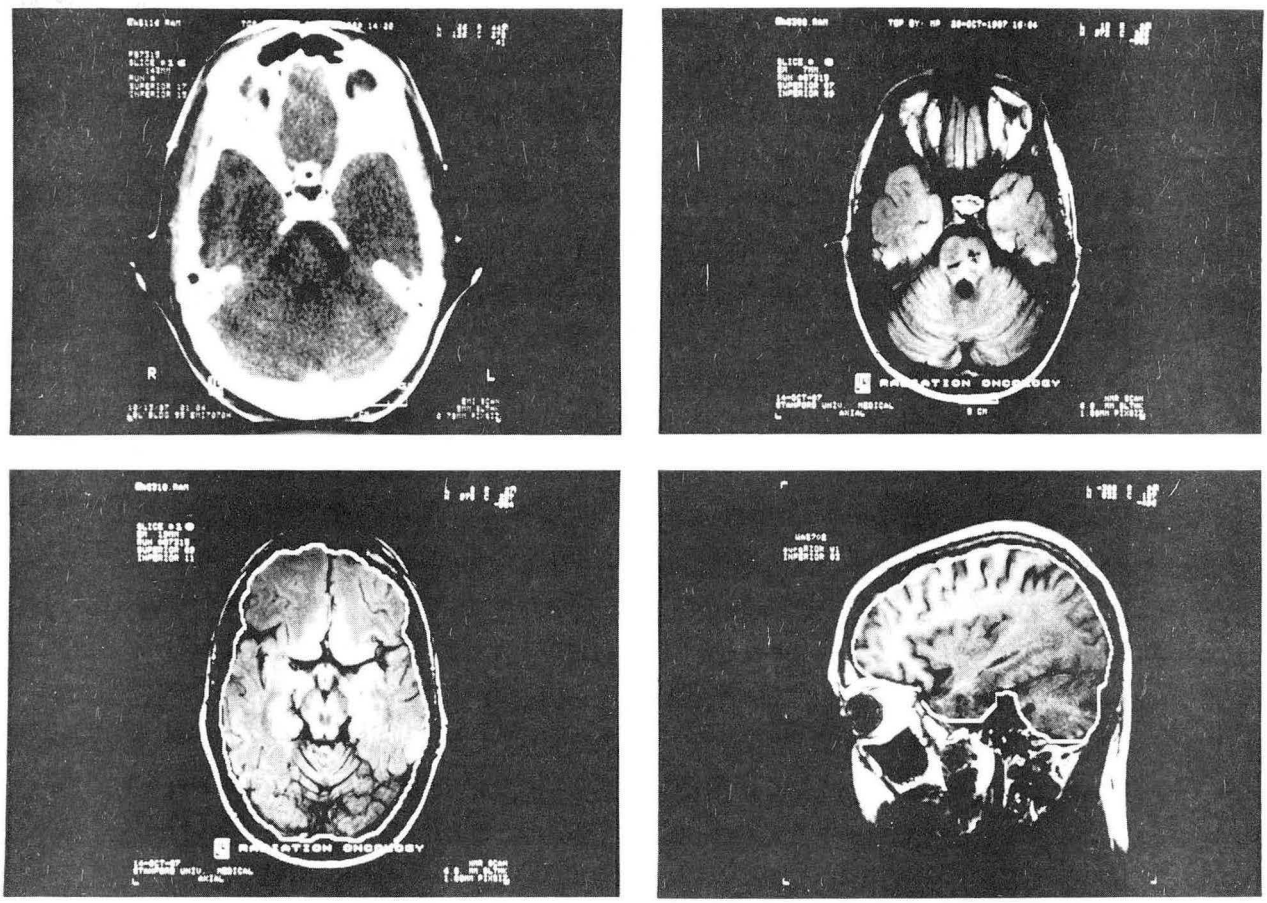

XBB 894-3702A

Fig. 1

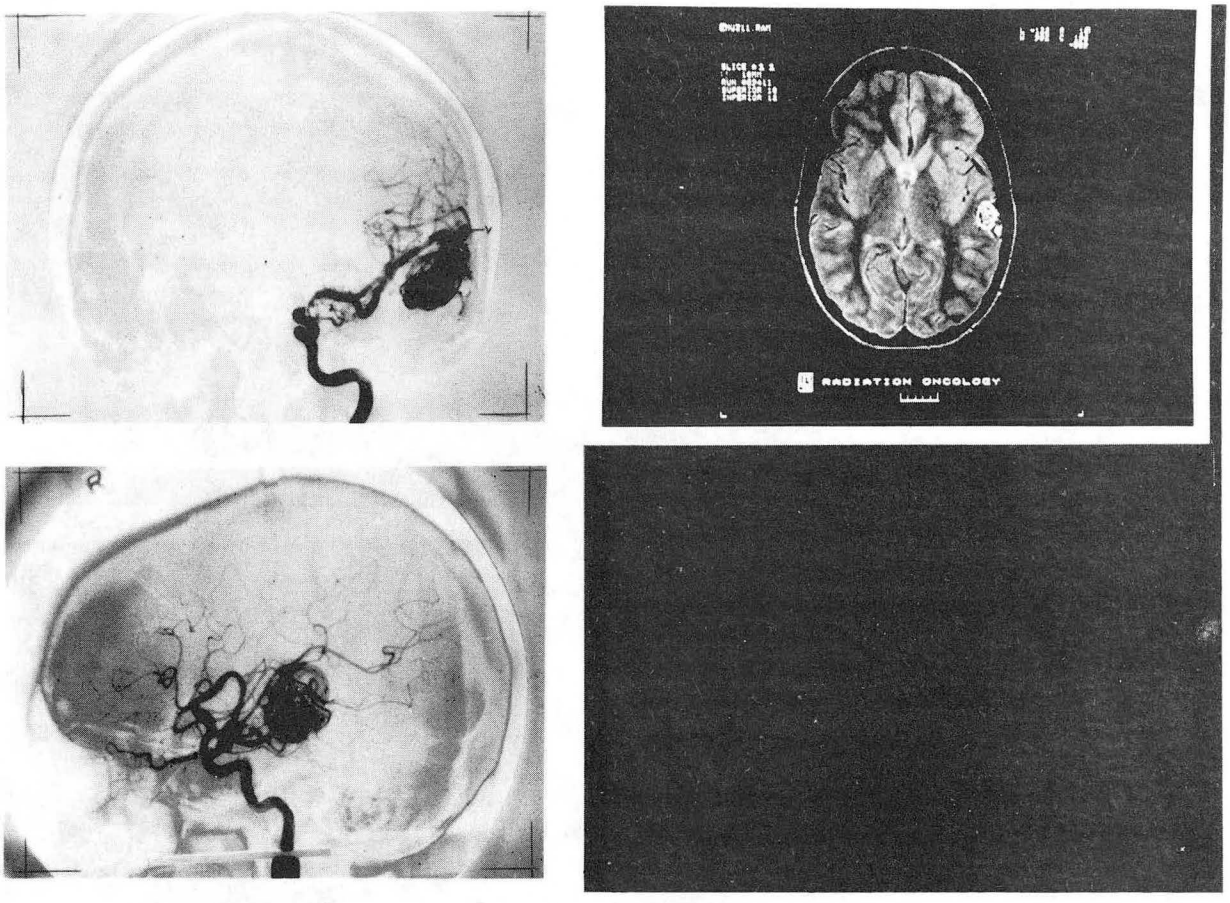

XBB 794-352-A

Fig. 2

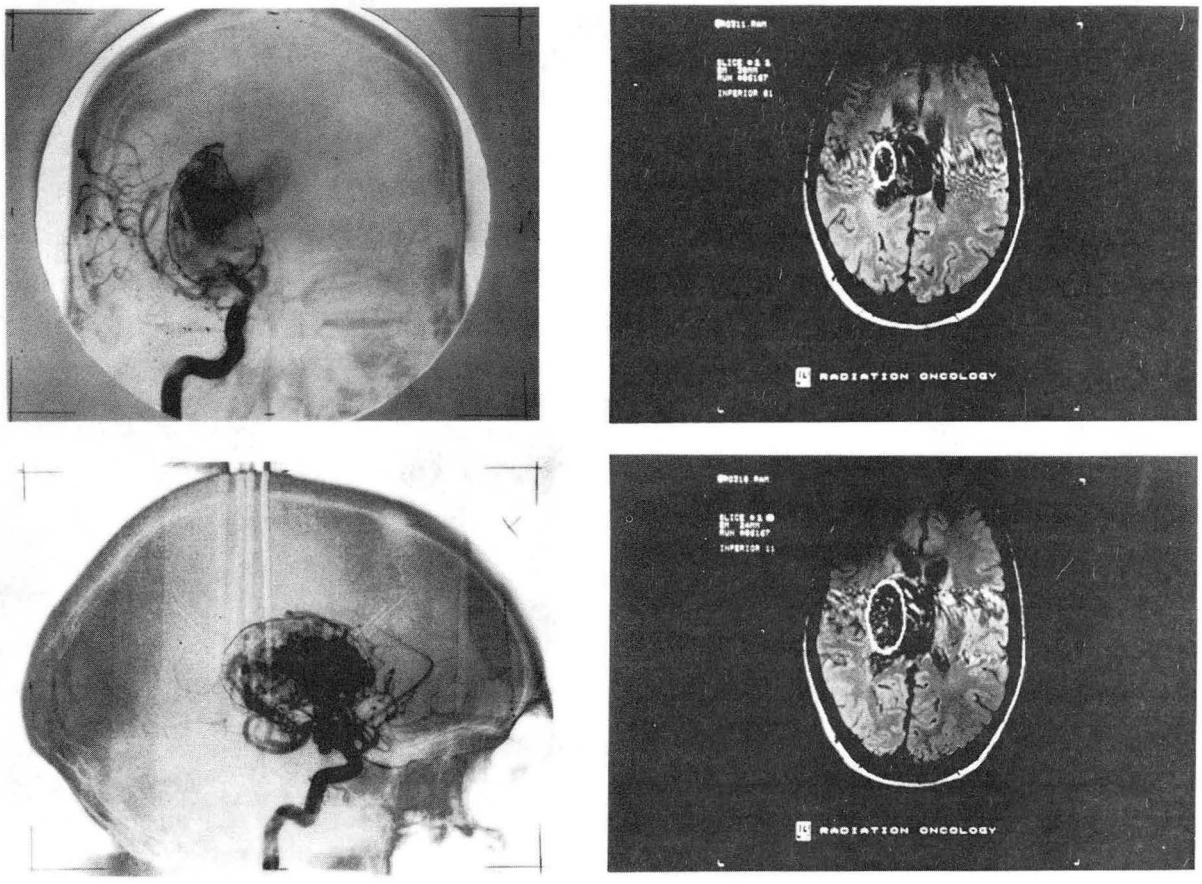

XBB 849-3523A

Fig. 3

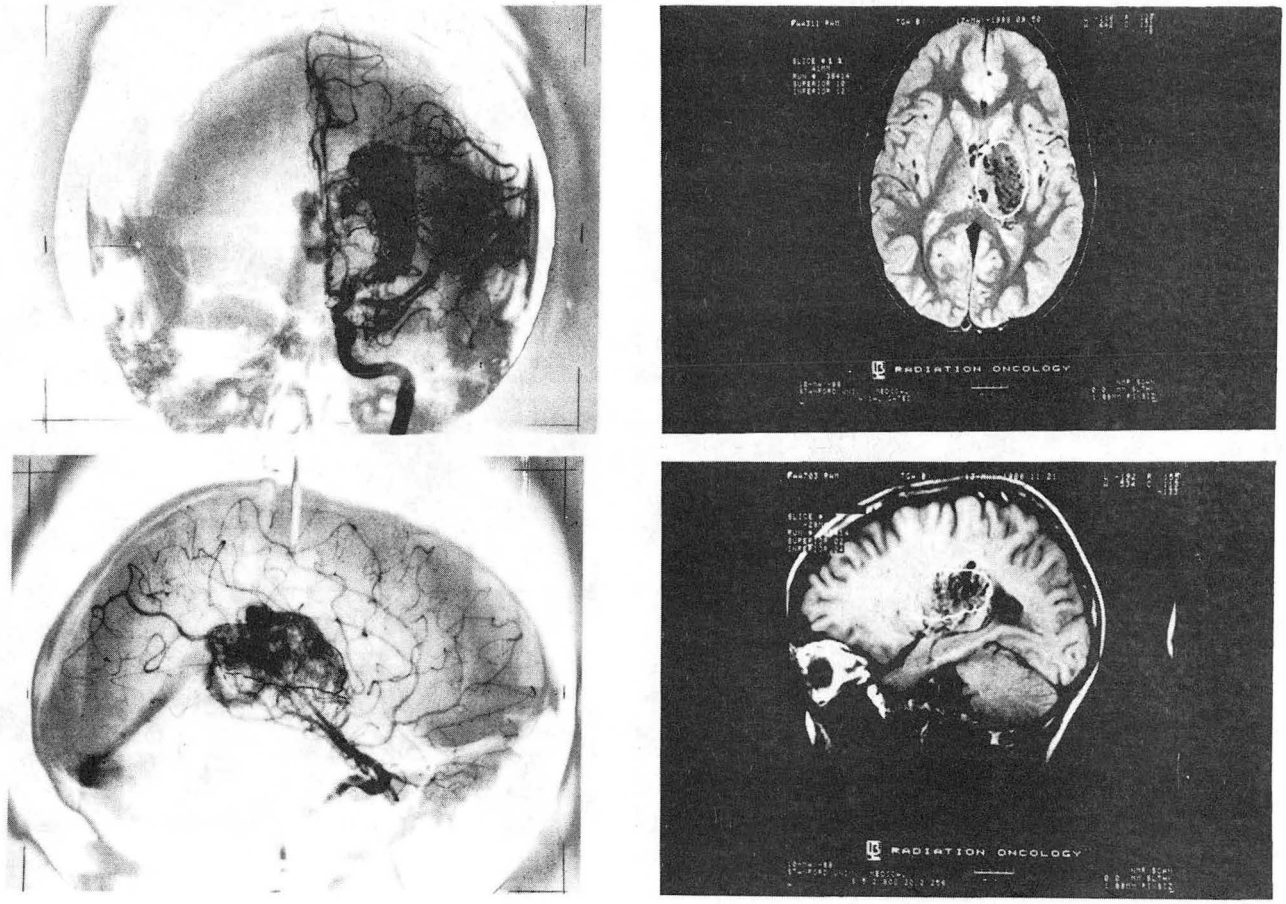

XBB 894-3524A

Fig. 4

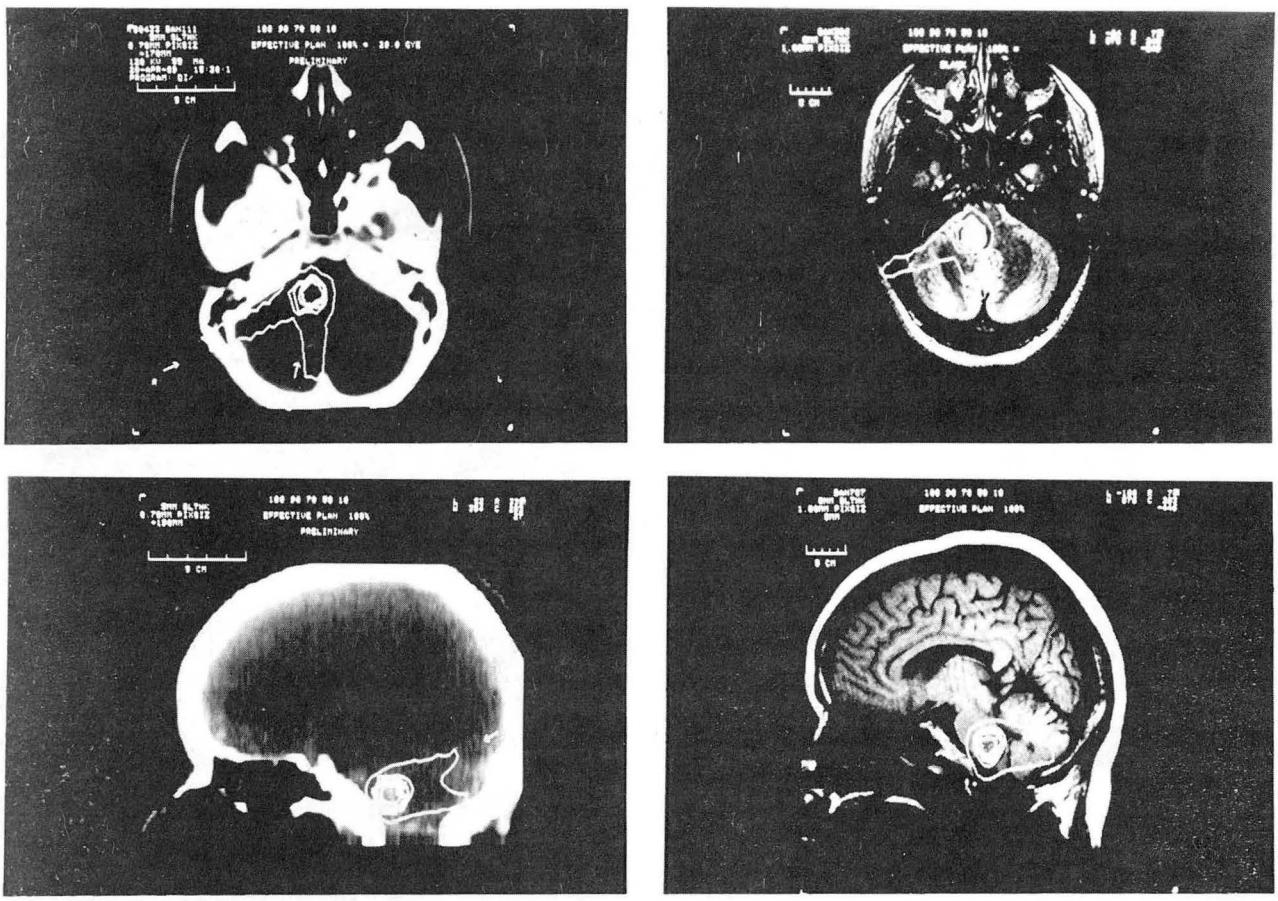

XBB 894-3712A

Fig. 5

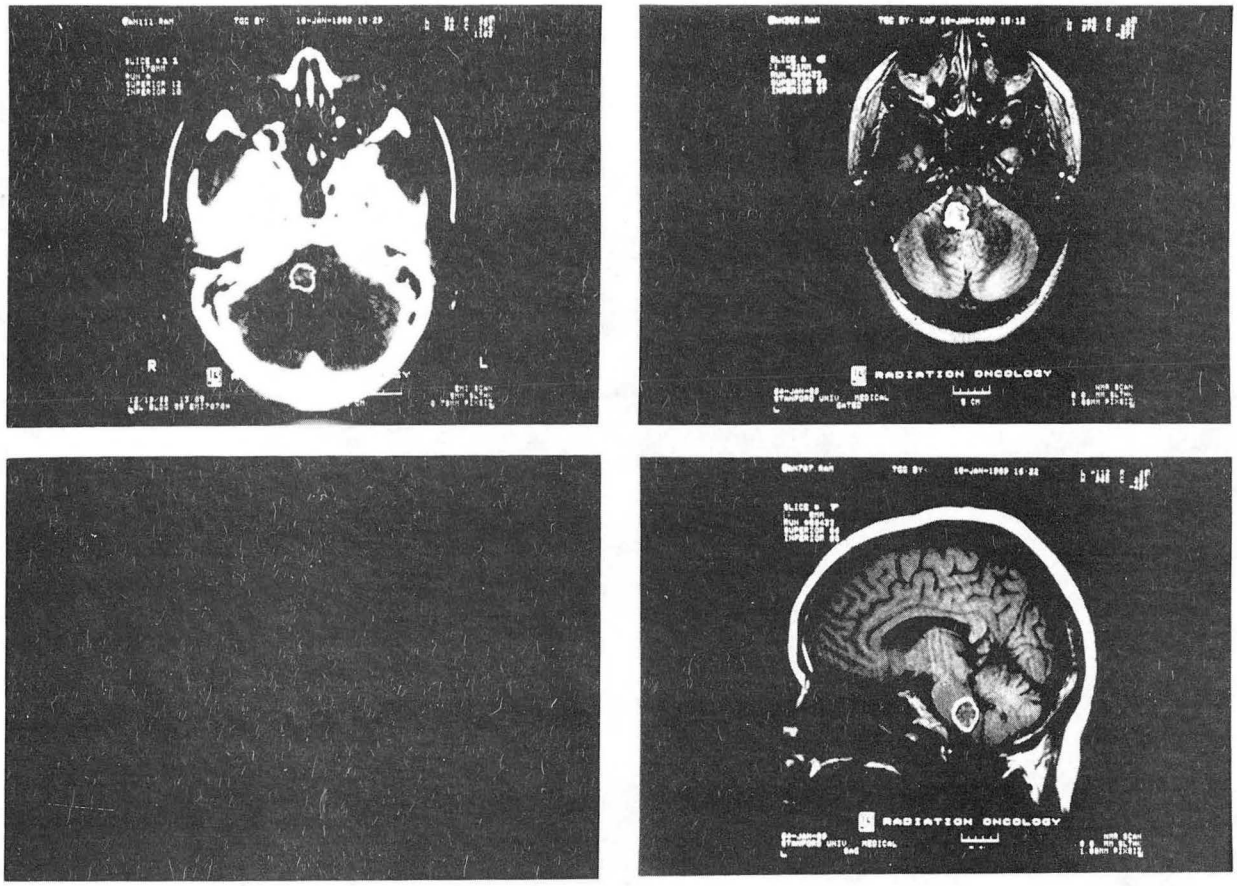

XBB 894-3707A

Fig. 6

LAWRENCE BERKELEY LABORATORY
TECHNICAL INFORMATION DEPARTMENT
1 CYCLOTRON ROAD
BERKELEY, CALIFORNIA 94720